Eur. Phys. J. B **27**, 541–547 (2002)
DOI: 10.1140/epjb/e2002-00187-8

THE EUROPEAN PHYSICAL JOURNAL B

Pattern formation in the A + B_2 reaction with anisotropic lateral adsorbate-adsorbate interactions

V.P. Zhdanov[1,2,a] and B. Kasemo[1]

[1] Department of Applied Physics, Chalmers University of Technology, 412 96 Göteborg, Sweden
[2] Boreskov Institute of Catalysis, Russian Academy of Sciences, Novosibirsk 630090, Russia

Received 4 January 2002 and Received in final form 2 April 2002
Published online 25 June 2002 –

Abstract. We present Monte Carlo simulations of the formation of (1×2) islands in the case of the $2A + B_2 \rightarrow 2AB$ reaction occurring *via* the Langmuir-Hinshelwood mechanism on a square lattice under steady-state conditions. The model employed takes into account the effect of anisotropic lateral B-B interactions on the rates of B diffusion and elementary reaction events. The results obtained with qualitatively realistic ratio of the rate of elementary reaction steps indicate that the average island size depends on the details of diffusion and reaction dynamics in a similar way as in the earlier studied case of the simplest $A + B$ reaction running *via* the Eley-Rideal mechanism.

PACS. 05.10.Ln Monte Carlo methods – 05.50.+q Lattice theory and statistics (Ising, Potts, etc.) – 05.70.Fh Phase transitions: general studies – 82.40.Np Temporal and spatial patterns in surface reactions

1 Introduction

Pattern formation (PF) in heterogeneous catalytic reactions may occur during transient regimes and also under steady-state conditions. In both cases, this phenomenon results from the interplay of reaction steps and adsorbate diffusion. The fact that transient kinetics (titration or temperature-programmed regimes) of rapid catalytic reactions are often accompanied by PF has long been recognized from numerous observations indicating that the dependence of the reaction rate on adsorbate coverage is frequently not unique, *i.e.*, the reaction kinetics are sensitive to the way how the adsorbed overlayer is prepared (for a brief review, see Ref. [1]). More recently, PF during titration has been observed explicitly in many systems by using scanning tunneling microscopy (STM) [2]. Theoretically, the transient reaction regimes accompanied by PF were analysed in references [1,3–5].

PF under steady-state conditions in the gas phase is more intriguing, because the conditions for coexistence of kinetic or thermodynamic phases can rarely be met. Often, this phenomenon is related to kinetic oscillations [6,7]. Non-oscillatory steady-state reaction regimes may be accompanied by PF as well. Experimental reports on such regimes are however scarce (for example, see STM studies [8] of CO oxidation on Cu(110)).

The shape of patterns, observed under steady-state conditions in the gas phase, and the ways how the patterns should be described depend on the intimate details of the behaviour of adsorbed particles. For example, patterns monitored in oscillatory reactions on the macroscopic scale (from μm up to mm) often exhibit wide smeared boundaries between the regions with domination of one or another species. Such patterns are customarily described by using the conventional mean-field (MF) reaction-diffusion equations [6] constructed in analogy with the mass-action equations widely employed for treating gas- and liquid-phase reactions [9]. In contrast, the boundaries of patterns observed on the mesoscopic scale (from a few nm to μm) are frequently atomically sharp. This feature is indicative of phase separation related to adsorbate-induced surface restructuring and/or adsorbate-adsorbate lateral interactions. The most appropriate tool for analysis of patterns of the latter type is the Monte Carlo (MC) technique.

The available MC simulations of PF occurring under steady-state conditions in the gas phase are focused primarily on oscillatory reaction regimes (for a review, see Ref. [10]). Patterns in non-oscillatory reactions were simulated in references [11–15] (for related phenomenological MF treatments, see Refs. [16,17]). In particular, the simplest Eley-Rideal $A + B$ reaction with A-A lateral interactions or A-induced surface restructuring was studied in detail in references [11–13] and [14], respectively.

In this paper, we will discuss PF due to adsorbate-adsorbate lateral interactions in the $A + B_2$ reaction. The standard mechanism of this reaction includes reversible monomolecular A adsorption,

$$A_{\rm gas} \rightleftharpoons A_{\rm ads}, \tag{1}$$

[a] e-mail: zhdanov@fy.chalmers.se

irreversible dissociative B_2 adsorption,

$$(B_2)_{\rm gas} \to 2B_{\rm ads}, \tag{2}$$

and the Langmuir-Hinshelwood (LH) step, resulting in the product formation,

$$A_{\rm ads} + B_{\rm ads} \to (AB)_{\rm gas}. \tag{3}$$

This scheme is well known to mimic CO oxidation on the noble metal catalysts Pt, Pd and Rh (A then stands for CO, and B_2 for O_2). The kinetics predicted on its basis are also representative for many other reactions [18]. For these reasons, the $A+B_2$ reaction has long attracted attention. In particular, the MF steady-state kinetics obtained on the basis of the reaction mechanism (1)-(2) are widely used already several decades in order to describe experiment (see the reviews [18,19]). The first MC simulations [20] of the $A + B_2$ reaction were focused on the case when adsorbed A and B species are immobile. Later on, the MC technique was widely employed to analyze different aspects of the reaction under consideration. In particular, the $A + B_2$ reaction scheme with lateral interactions was treated in references [21–23] (for the review, see Sect. 5.1 in Ref. [18] and Sect. 2.2.1 in Ref. [24]). The latter studies (Refs. [21–23]) were however focused rather on the kinetic phase diagrams than on PF. More recently, the formation of B islands in the $A+B_2$ reaction with isotropic attractive B-B lateral interactions was simulated in reference [15].

The results obtained in references [11–15] indicate that the size and shape of patterns in catalytic reactions are sensitive to the details of the diffusion and reaction dynamics. To extend the understanding the problem under consideration, we present MC simulations of PF in the $A+B_2$ reaction with strongly anisotropic B-B lateral interactions resulting in the formation of (1×2) islands. This case is of interest from the point of view of both theory and experiment. Indeed, although anisotropic lateral interactions are common on the (110) face of fcc metals, the specifics of PF in catalytic reactions with such interactions was so far not clear.

2 Specification of the model

In our simulations, the $A + B_2$ reaction is run on a square $(L \times L)$ lattice with periodic boundary conditions. A and B_2 adsorption occur on vacant sites and pairs of nearest-neighbour (nn) vacant sites, respectively. Reaction (3) between nn A and B particles is allowed if they are located in nn sites. A and B diffusion is realized *via* jumps to vacant nn sites. Reaction (3) is considered to be rapid compared to A and B_2 adsorption and A desorption and slow compared to A and B diffusion (this is often the case in real systems [15]).

In general, the rates of the reaction steps may depend on A-A, B-B and A-B lateral interactions. Our present simulations are focused on the B-B interactions. Specifically, we take into account nn B-B interactions in the X and Y directions, ϵ_1^x and ϵ_1^y, and next-nn B-B interaction in the X direction, ϵ_2^x. The interactions ϵ_1^y and ϵ_2^x are assumed to be attractive (negative). The interaction ϵ_1^x is considered to be repulsive (positive). The other interactions are ignored. With this choice of parameters, B particles have tendency to form a (1×2) structure oriented along the Y direction. This type of ordering is common for oxygen adsorption on the (110) face of fcc metals. In reality, the formation of the (1×2) structure is often related to spontaneous or adsorbate-induced surface restructuring. In our simulations, surface restructuring is not treated explicitly. Nevertheless, the results obtained may be applicable to real systems with surface restructuring, because if this process is relatively rapid it can be mimicked implicitly by assuming the B-B lateral interactions to be effective.

To incorporate the influence of the B-B lateral interactions on the rates of the LH reaction and B diffusion, we recall that according to the transition state theory the rate constant of an elementary rate process for a given arrangement of adjacent particles is represented as [25]

$$k_i = k_\circ \exp[-(\epsilon_i^* - \epsilon_i)/k_{\rm B}T], \tag{4}$$

where $k_\circ$ is the rate constant corresponding to the low-coverage limit, ϵ_i and ϵ_i^* are the lateral interactions in the initial and activated states, and i is the subscript characterizing the arrangement. Equation (4) is applicable both to diffusion and reaction. Depending on the choice of the interaction ϵ_i^*, it makes it possible to describe very different types of diffusion and reaction dynamics.

In our work, we use for B diffusion the standard Metropolis (MP) dynamics with the normalized jump probability given by

$$P_i^{\rm dif} = \begin{cases} 1 & \text{for } \epsilon_f \le \epsilon_i, \text{ and} \\ \exp[-(\epsilon_f - \epsilon_i)/k_{\rm B}T] & \text{for } \epsilon_f > \epsilon_i, \end{cases} \tag{5}$$

where ϵ_f is the energy of the final state, and also more realistic "initial-state" dynamics,

$$P_i^{\rm dif} = \exp[(\epsilon_i - 2\epsilon_1^x)/k_{\rm B}T], \tag{6}$$

often used in simulations of surface diffusion [25,26]. In both cases, the jump probability is defined so that the maximum probability is equal to unity (to satisfy this condition, we substract $2\epsilon_1^x$ from ϵ_i in Eq. (6)).

For the LH step (3), the lateral interaction in the activated state is assumed to be a fraction of that in the ground state, *i.e.*, $\epsilon_i^* = (1-\alpha)\epsilon_i$, where $\alpha \le 1$. In this case, the normalized reaction probability can be represented as

$$P_i^{\rm rea} = \exp[\alpha(\epsilon_i - 2\epsilon_1^x)/k_{\rm B}T]. \tag{7}$$

According to this definition, the maximum reaction probability is equal to unity. The simulations have been performed for $\alpha = 0$ and 0.5.

In MC simulations, the rate constants of different events should be normalized to an arbitrary chosen rate constant which is equal to or larger than the maximum

rate possible for reacting particles [27]. In our model (see below), the maximum rate is given by $k_{\max} = k_{\rm des} + k_{\rm LH} + k_{\rm dif}$, where $k_{\rm des}$, $k_{\rm LH}$ and $k_{\rm dif}$ are the rate constants for A desorption, LH reaction, and diffusion, respectively. To simulate the reaction kinetics, we use $k_{\max}$ for normalization. In particular, we introduce the dimensionless parameter, $p_{\rm rea} \equiv (k_{\rm des} + k_{\rm LH})/k_{\max}$, characterizing the relative rates of the catalytic cycle (steps (1–3)) and adsorbate diffusion. The rates of these processes are considered to be proportional to $p_{\rm rea}$ and $1 - p_{\rm rea}$, respectively. More specifically, we employ the number $N_{\rm dif} \equiv (1 - p_{\rm rea})/p_{\rm rea}$ characterizing the ratio of the rates of diffusion and reaction. Taking into account that adsorbate diffusion is usually fast compared to reaction, we should have $N_{\rm dif} \gg 1$. The bulk of simulations described below was executed for $N_{\rm dif} = 10^3$. The number of diffusion trials per A and B particle was considered to be equal. In reality, A (CO) diffusion is much faster than B (O) diffusion. In the simulations, B diffusion is slowed down due to attractive B-B lateral interactions. For this reason, A diffusion is anyway rapid compared to B diffusion, and A particles are distributed nearly at random. Under such circumstances, there is no need to employ a higher number of diffusion trials for A particles.

Inside the catalytic cycle, the rates are normalized to $k_{\rm des} + k_{\rm LH}$. Specifically, the rates of A and B_2 adsorption and A desorption are considered to be proportional to $p_A \equiv k_A P_A/(k_{\rm des} + k_{\rm LH})$, $p_{B_2} \equiv k_{B_2} P_{B_2}/(k_{\rm des} + k_{\rm LH})$ and $p_{\rm des} \equiv k_{\rm des}/(k_{\rm des} + k_{\rm LH})$ ($k_A P_A$ and $k_{B_2} P_{B_2}$ are the A and B_2 impingement rates). The rate of the LH step (3) is proportional to $1 - p_{\rm des}$.

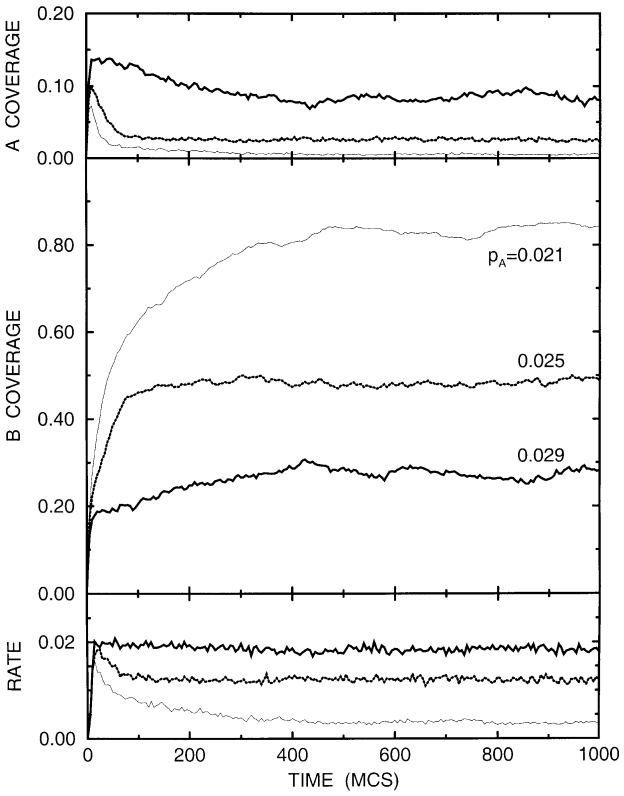

Fig. 1. Adsorbate coverages (ML (ML ≡ monolayer)) and reaction rate (MC/MCS) as a function of time for the MP diffusion dynamics and reaction dynamics with $\alpha = 0$ and $p_A = 0.021$ (thin solid lines), 0.025 (dotted lines), and 0.029 (thick solid lines). The other parameters are standard ($\epsilon_1^x/k_{\rm B}T = 1$, $\epsilon_1^y/k_{\rm B}T = -3$, $\epsilon_2^x/k_{\rm B}T = -1$, $p_A + p_{B_2} = 0.05$, $p_{\rm des} = 0.002$, $N_{\rm dif} = 10^3$, and $L = 100$). The time interval between data points is 5 MCS. The reaction rate is calculated as average over 5 MCS.

3 Algorithm of simulations

Reaction or diffusion steps occur in parallel. To simulate these steps, one can choose one of the MC algorithms described in reference [27]. With the specification above (Sect. 2), our MC algorithm is as follows:

(1) A random number ρ ($0 \le \rho \le 1$) is generated. If $\rho > p_{\rm rea}$, a diffusion trial is performed (item (2)). If $0 < \rho < p_{\rm rea}$, a reaction trial is executed (item (3)).

(2) For diffusion, an adsorption site is chosen at random. If the site is vacant, the trial ends. Otherwise, an A or B particle located in this site tries to diffuse. In particular, an adjacent site is randomly selected, and if the latter site is vacant, an A particle is replaced into it. For a B particle, a new random number ρ' ($0 \le \rho' \le 1$) is generated, and then the replacement to the vacant site is performed if $\rho' \le P_i^{\rm dif}$, where $P_i^{\rm dif}$ is the probability defined by equation (5) or (6).

(3) A reaction trial contains several steps. (i) An adsorption site is chosen at random. (ii) A new random number ρ' ($0 \le \rho' \le 1$) is generated. (iii) If the site selected is vacant, A or B_2 adsorption acts are realized provided that $\rho' < p_A$ and $p_A < \rho' < p_A + p_{B_2}$, respectively (if $\rho' > p_A + p_{B_2}$, the trial ends). For B_2 adsorption, one of the nn sites is chosen at random, and the trial is accepted provided that the latter site is vacant. (iv) If the site selected is occupied by A, A desorption or reaction act is executed for $\rho' < p_{\rm des}$ and $\rho' > p_{\rm des}$, respectively. For A reaction, one of the nn sites is chosen at random. If the latter site is occupied by B, reaction is performed with the probability $P_i^{\rm rea}$, given by equation (6). (v) If the site selected is occupied by B, the trial ends.

All the MC runs were started from the clean surface. To measure time, we use MC steps (MCS). One MCS is defined as $L \times L$ attempts of the adsorption-reaction events, *i.e.*, to calculate MC time, the total number of MC trials is multiplied by $p_{\rm rea}$ and divided by $L \times L$. This means that the MC and real times are interconnected as $t_{\rm MC} = (k_{\rm des} + k_{\rm LH})t$. (In principle, one might define one MCS as $L \times L$ trials of adsorption, reaction, and diffusion. In the latter case, the time scale would primarily be connected with diffusion, because in our simulations this process is rapid compared to other steps. In experiment, time is usually related to reaction steps. For this reason, we also prefer to employ the time scale connected with the catalytic cycle.)

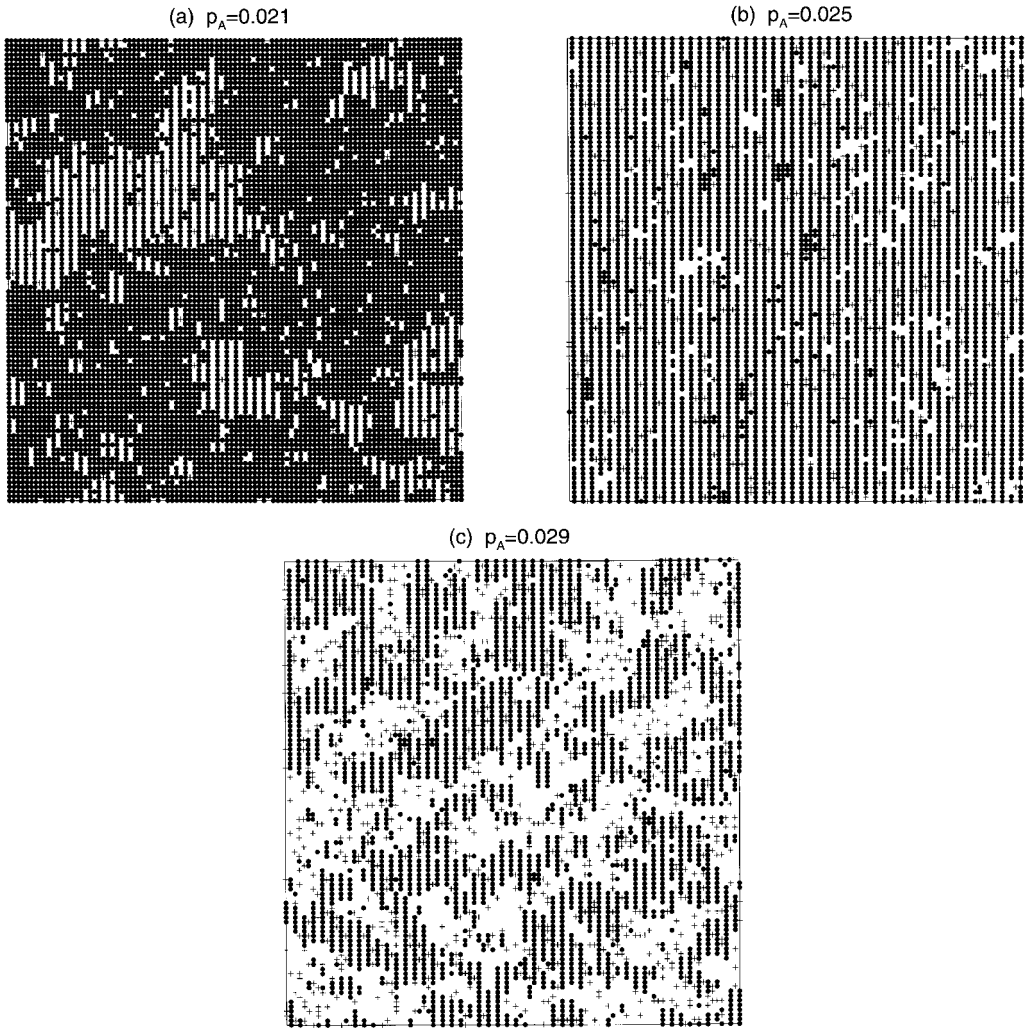

Fig. 2. Snapshots of the lattice in the end of the MC runs shown in Figure 1. Plus signs and filled circles represent A and B particles respectively.

4 Results of simulations

The simulations were executed on a lattice with $L = 100$ at temperatures below the critical temperature. Specifically, we use $\epsilon_1^x/k_{\rm B}T = 1$, $\epsilon_1^y/k_{\rm B}T = -3$, $\epsilon_2^x/k_{\rm B}T = -1$. The values of the kinetic parameters were chosen in qualitative agreement with the data available for real systems (see, *e.g.*, the discussion in Ref. [15]). In particular, A and B_2 adsorption were considered to be faster than A desorption and slower than the LH step, which in turn was assumed to be slow compared to adsorbate diffusion (in reality, the latter is fulfilled for A diffusion but not always the case for B diffusion). To satisfy these conditions, we employ $p_A + p_{B_2} = 0.05$, $p_{\rm des} = 0.002$, $N_{\rm dif} = 10^3$, and $L = 100$. With this choice, the appropriate governing parameter is p_A. The duration of MC runs was as a rule 10^3 MCS (see, *e.g.*, Fig. 1). This time is sufficient in order to reach steady state.

Under steady-state conditions with the parameters above, the surface is almost completely covered by B at $p_A < 0.02$. At $p_A > 0.03$, the B coverage is usually low. The formation of mesoscopic (1×2) B islands occurs at $0.02 \leq p_A \leq 0.03$. Typical islands obtained for the MP diffusion dynamics and reaction dynamics with $\alpha = 0$ are shown in Figure 2. For $p_A = 0.021$, the B coverage is relatively high (Fig. 1), and one can observe (1×2) B islands in the (1×1) B sea (Fig. 2a). At $p_A = 0.025$, the B coverage is close to 0.5, and the adsorbed overlayer is in the almost perfect (1×2) state (Fig. 2b). For $p_A = 0.029$, the B coverage is relatively low, and the (1×2) B islands coexist with nearly empty regions (Fig. 2c).

Typical (1×2) patterns observed during MC runs with the MP diffusion dynamics and reaction dynamics with $\alpha = 0.5$ are exhibited in Figure 3. For this reaction dynamics, due to B-B lateral interactions, the reaction probability (Eq. (6)) inside (1×2) islands is lower than that on the island boundaries or in the case of single A-B pairs.

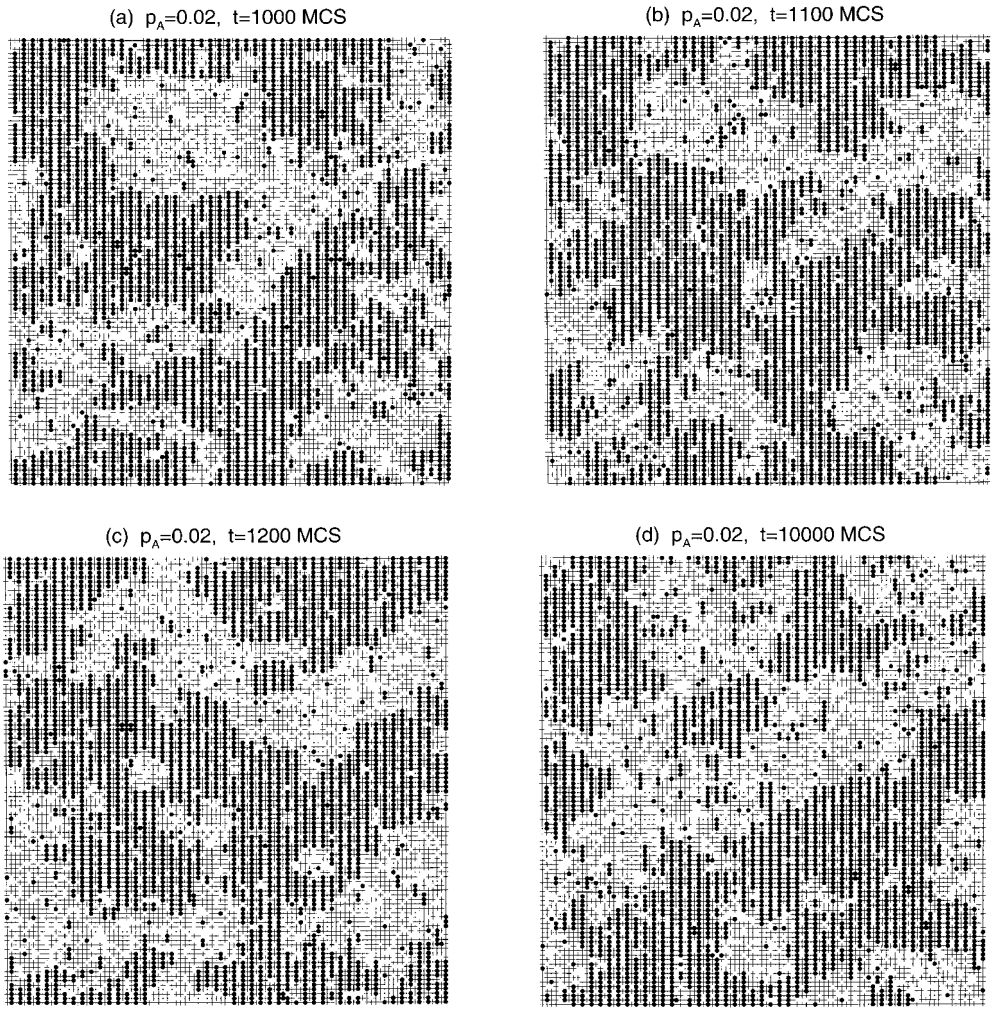

Fig. 3. Snapshots of the lattice during a MC run with the MP diffusion dynamics and reaction dynamics with $\alpha = 0.5$ and $p_A = 0.022$ (the other parameters are as in Fig. 1). In this case, the steady-state A and B coverages and reaction rate are $\simeq$0.48 ML, 0.28 ML, and 0.0042 ML/MCS, respectively. The designations are as in Figure 2.

This facilitates the island formation. For this reason, the average island size becomes larger (*cf.* Figs. 2c and 3a). In addition, the A coverage increases. To illustrate the spatio-temporal behaviour of the (1×2) islands, the lattice snapshots (Fig. 3) are shown at $t = 1000$, 1100, 1200, and 10000 MCS. The average reaction rate during this run is about 0.004 ML/MCS. This means that the time interval of 100 MCS corresponds to reaction of 0.4 ML of A (or B) particles. The change of islands during this time interval is appreciable (*cf.* Figs. 3a and b). After 200 MCS, the shift of islands is comparable with their size (*cf.* Figs. 3a and c). This indicates that the islands are traveling.

For the initial-state diffusion dynamics and reaction dynamics with $\alpha = 0$, the (1×2) islands are appreciably smaller (*cf.* Fig. 4a–c and Figs. 2 and 3). This effect is qualitatively similar to that observed earlier in the $A + B$ reaction [11,13]. Quantitatively, the influence of the details of the diffusion dynamics on the formation of islands is stronger for the latter reaction. In both cases, the decrease of the average island size is connected with the fact that according to the initial-state diffusion dynamics the difference of the rates of particle jumps inside and outside islands is larger compared to that for the MP dynamics. This makes it more difficult to balance the diffusion fluxes inside and outside the islands. With increasing diffusion rate by one order of magnitude, the average island size becomes larger (*cf.* Figs. 4c and d) but only slightly (by a factor of 2). This result is in line with the Lifshits-Slozov law predicting that the dependence of the average island size on the diffusion coefficient is relatively weak, $R \propto D^{1/3}$ (see, *e.g.*, Chap. 5 in Ref. [25]). (Although this law is not directly applicable at chemically reactive conditions, it makes it possible to understand qualitatively what occurs in this case.)

For the initial-state diffusion dynamics and reaction dynamics with $\alpha = 0.5$, the average island size is larger than for $\alpha = 0$ (*cf.* Figs. 4c and 5) but smaller than for

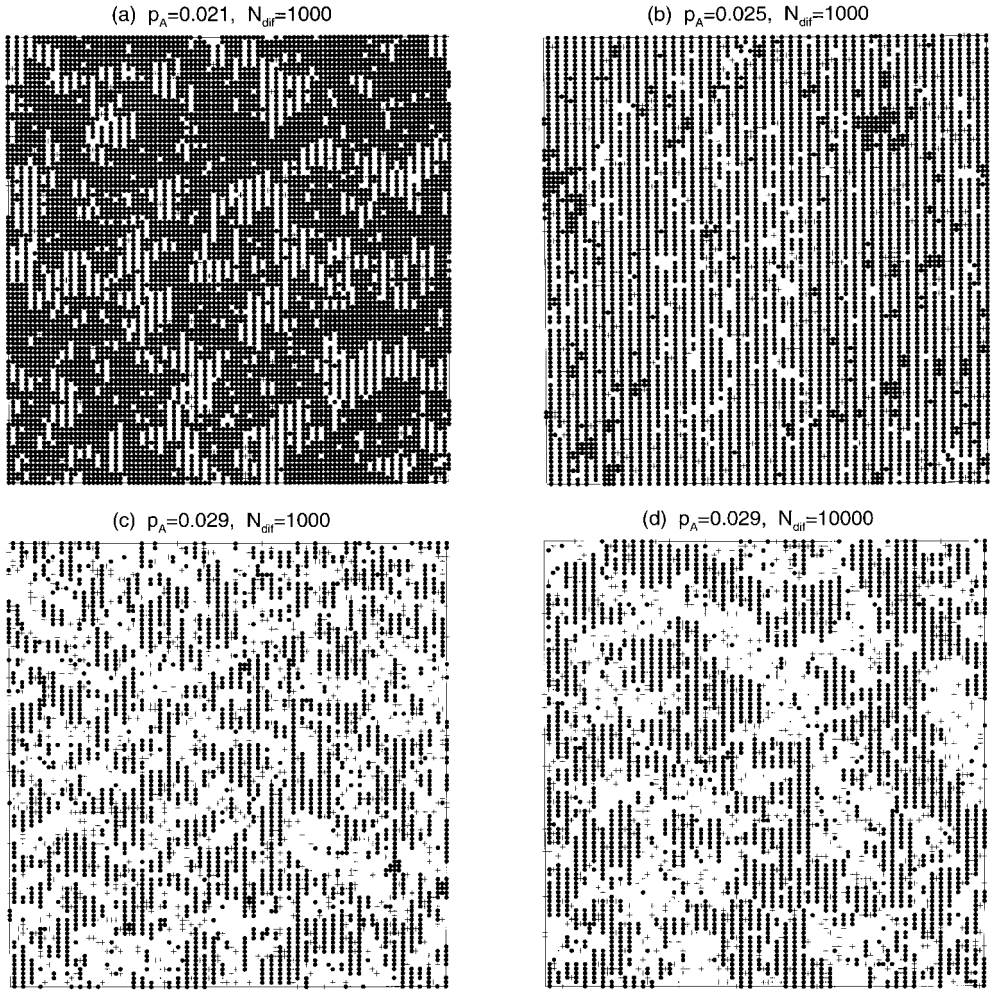

Fig. 4. Typical snapshots of the lattice at $t = 1000$ MCS for the initial-state diffusion dynamics and reaction dynamics with $\alpha = 0$ for (a-c) $p_A = 0.021$, 0.025, 0.029 and $N_{\rm dif} = 10^3$, and (d) $p_A = 0.029$ and $N_{\rm dif} = 10^4$ (the other parameters are as in Fig. 1). The designations are as in Figure 2.

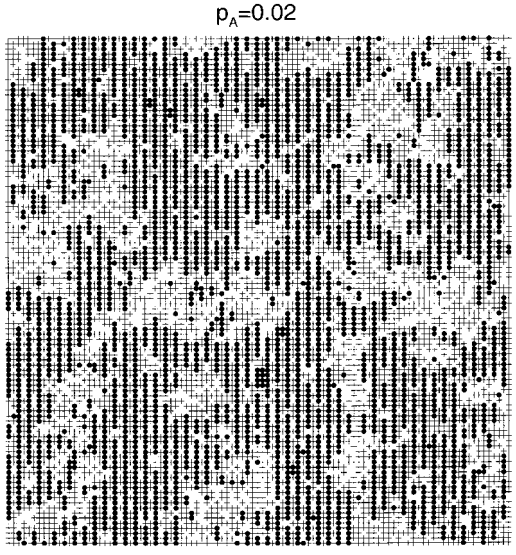

Fig. 5. Typical snapshots of the lattice at $t = 1000$ MCS for the initial-state diffusion dynamics and reaction dynamics with $\alpha = 0.5$ for $p_A = 0.02$ (the other parameters are as in Fig. 1).

the MP diffusion dynamics and reaction dynamics with $\alpha = 0.5$ (*cf.* Figs. 3 and 5).

5 Conclusion

We have shown the effect of the details of diffusion and reaction dynamics on the formation of (1×2) patterns during the the $A + B_2$ reaction with strongly anisotropic lateral adsorbate-adsorbate interactions. Although the reaction scheme and the type of adsorbate ordering are quite different in this case compared to those for the $A+B$ reaction [11,13], the qualitative conclusions are similar in both cases. In particular, the implementation of the initial-state diffusion dynamics always results in much smaller islands compared to those corresponding to the conventional MP dynamics. Thus, we may conclude that despite the dependence of the pattern formation on the details of diffusion and reaction dynamics, there exist some general principles behind this phenomenon.

This work was supported by the NUTEK Competence Center for Catalysis at Chalmers University of Technology (grant No 4F7-97-10929).

References

1. B. Hellsing, V.P. Zhdanov, Chem. Phys. Lett. **147**, 613 (1988)
2. J. Wintterlin, Adv. Catal. **45**, 131 (2000)
3. M. Silverberg, A. Ben-Shaul, F. Rebentrost, J. Chem. Phys. **83**, 6501 (1985)
4. V.P. Zhdanov, Phys. Rev. Lett. **77**, 2109 (1996)
5. S. Völkening, J. Wintterlin, J. Chem. Phys. **114**, 6382 (2001)
6. R. Imbihl, G. Ertl, Chem. Rev. **95**, 697 (1995)
7. H.H. Rotermund, Surf. Sci. Rep. **29**, 265 (1997)
8. W.W. Crew, R.J. Madix, Surf. Sci. **349**, 275 (1996)
9. *Chemical Waves and Patterns*, edited by R. Kapral, K. Showalter (Kluwer, Dordrecht, 1994)
10. V.P. Zhdanov, Surf. Sci. Rep. **45**, 231 (2002)
11. V.P. Zhdanov, Surf. Sci. **392**, 185 (1997)
12. V.P. Zhdanov, Surf. Sci. **401**, 412 (1998)
13. V.P. Zhdanov, Langmuir **17**, 1793 (2001)
14. V.P. Zhdanov, Surf. Sci. **486**, L513 (2001)
15. V.P. Zhdanov, B. Kasemo, Surf. Sci. **412**, 527 (1998)
16. M. Hildebrand, A.S. Mikhailov, G. Ertl, Phys. Rev. Lett. **81**, 2602 (1998)
17. M. Hildebrand, M. Kuperman, H. Wio, A.S. Mikhailov, G. Ertl, Phys. Rev. Lett. **83**, 1475 (1999)
18. V.P. Zhdanov, B. Kasemo, Surf. Sci. Rep. **20**, 111 (1994)
19. L.F. Razon, R.A. Schmitz, Catal. Rev. Sci. Eng. **28**, 89 (1986)
20. R.M. Ziff, E. Gulari, Y. Barshad, Phys. Rev. Lett. **56**, 2553 (1986)
21. H.-P. Kaukonen, R.M. Nieminen, J. Chem. Phys. **91**, 4380 (1989)
22. J.-J. Luque, F. Jinenez-Morales, M.C. Lemos, J. Chem. Phys. **96**, 8535 (1992)
23. J. Satulovsky, E.V. Albano, J. Chem. Phys. **97**, 9440 (1992)
24. E.V. Albano, Heter. Chem. Rev. **3**, 389 (1996)
25. V.P. Zhdanov, *Elementary Physicochemical Processes on Solid Surfaces* (Plenum, New York, 1991), Chaps. 4, 5 and 7
26. F. Nieto, A.A. Tarasenko, C. Uebing, Def. Diffus. Forum **162**, 59 (1998)
27. K. Binder, in *Monte Carlo Methods in Statistical Physics*, edited by K. Binder (Springer, Berlin, 1979), p. 1